

Trends in COVID-19 prevalence and mortality: a year in review

Nick James^a, Max Menzies^b

^a*School of Mathematics and Statistics, University of Sydney, NSW, Australia*
^b*Yau Mathematical Sciences Center, Tsinghua University, Beijing, China*

Abstract

This paper introduces new methods to study the changing dynamics of COVID-19 cases and deaths among the 50 worst-affected countries throughout 2020. First, we analyse the trajectories and turning points of rolling mortality rates to understand at which times the disease was most lethal. We demonstrate five characteristic classes of mortality rate trajectories and determine structural similarity in mortality trends over time. Next, we introduce a class of *virulence matrices* to study the evolution of COVID-19 cases and deaths on a global scale. Finally, we introduce *three-way inconsistency analysis* to determine anomalous countries with respect to three attributes: countries' COVID-19 cases, deaths and human development indices. We demonstrate the most anomalous countries across these three measures are Pakistan, the United States and the United Arab Emirates.

Keywords: COVID-19, Time series analysis, Nonlinear dynamics, Anomaly detection

1. Introduction

2020 will be remembered as the year that the world first battled the COVID-19 pandemic. Almost 2 million people lost their lives, substantial restrictions on population movement and activities were imposed, and almost every country experienced an economic recession. During that year, treatments improved substantially [1, 2, 3, 4] and several vaccines were produced by the end of the year [5, 6]. However, the disease remains highly prevalent around the world as of the start of 2021, and measures to contain and reduce its transmission remain highly relevant for the reduction of casualties as well as economic and other social consequences [7, 8].

Throughout the year, government responses to the pandemic varied substantially, both over time and between countries. Early government responses included banning travel [9], the implementation of testing and contact tracing

Email address: `nicholas.james@sydney.edu.au` (Nick James)

programs [10], and lockdowns. Due to the economic consequences of lockdowns, many countries implemented them too late [11, 12] and lifted restrictions before cases had sufficiently reduced [13]. Such disparate responses to the virus led to great variability in case and death counts, creating *different waves* of the outbreak across many countries. Such later waves often exhibited higher case and death counts than the first [14, 15].

Close analysis of the dynamics of the disease on a country-by-country basis and over time is necessary to inform governments of the most successful strategies for reducing transmission of cases and progression to deaths. Identifying structural similarities between countries' trajectories can support conclusions that certain government responses will likely result in better or worse outcomes. Moreover, identifying anomalous countries can provide insights on which responses to the pandemic were exceptionally good or poor.

We implement new and existing time series analysis methods to analyse COVID-19 prevalence and mortality trends, both on a country-by-country basis and globally, with the identification of similarity and anomalies as our focus. Time series analysis has been applied broadly in epidemiology, including to studies of Ebola [16, 17], the Zika virus [18, 19], and more recently, COVID-19 itself [20, 21, 22, 23, 24]. Within the nonlinear dynamics community, methods such as networks [25, 26], distance analysis [15, 27, 28, 29, 30] and power-law models [23, 20, 31] have been used to model physical phenomena in other contexts.

This paper is structured as follows. In Section 2, we analyse the trajectories of mortality rates on a country-by-country basis. In particular, we build upon a recently introduced algorithmic framework to identify the *turning points* of the mortality trajectories, which reveal when the disease was most and least lethal (with respect to the progression from cases to deaths). Then, we suitably modify existing semi-metrics to assign countries into classes of mortality trajectories. In Section 3, we analyse the eigenspectra of a new class of *virulence matrices* to study trends in the worldwide prevalence and mortality of COVID-19. In Section 4, we compare countries' case and death counts with their *human development index (HDI)* and use a new method to identify the most anomalous countries between these attributes. We believe that this is the first paper to quantitatively combine these features and identify respective anomalies. In Section 5, we summarise our findings regarding COVID-19 trends throughout the year 2020.

2. Mortality rate analysis

In this section, we study the dynamics of the COVID-19 mortality rate among $n = 50$ countries. Our data spans 01/01/2020 to 31/12/2020, a period of $T = 366$ days. We choose the countries with the 50 greatest total case counts of COVID-19 as of 31/12/2020, order these by alphabetical order, and index them $i = 1, \dots, n$. Let $x_i(t), y_i(t) \in \mathbb{R}$ be the multivariate time series of new daily cases and deaths, respectively, for $i = 1, \dots, n$ and $t = 1, \dots, T$. For a given country, let

$r_i(t)$ be its 30-day rolling mortality rate, defined by

$$r_i(t) = \frac{\sum_{s=t-29}^t y_i(s)}{\sum_{s=t-29}^t x_i(s)}, t = 30, \dots, T, \quad (1)$$

or zero if no cases have been observed over the last 30 days. This gives a multivariate time series $r_i(t)$, for $i = 1, \dots, n$ and $t = 30, \dots, T$. The data point at time t describes the rolling mortality rate over the prior 30 days.

2.1. Methodology

The aim of this section is to study these mortality trends on a country-by-country basis and identify structural similarity across different countries. For this purpose, we use two (semi)-metrics between the mortality rate time series and apply *hierarchical clustering* [32, 33] to these measures. Hierarchical clustering has been used in several epidemiological applications, including inflammatory diseases [34], airborne diseases [35], Alzheimer's disease [36], Ebola [37], SARS [38], and COVID-19 [21].

These mortality rates $r_i(t)$ exhibit highly undulating behaviour, moving between clear peaks and troughs (turning points). Our first semi-metric measures distance between algorithmically-identified turning points as a proxy for each time series' behaviour. We modify an existing algorithmic framework for this purpose. First, we apply a *Savitzky-Golay filter* to produce a collection of smoothed time series $\hat{r}_i(t)$, $t = 30, \dots, T$ and $i = 1, \dots, n$. Next, we follow [15] and apply a two-step algorithm where we select and then refine a set of turning points. We assign each smoothed mortality rate time series a non-empty set P_i and T_i of local maxima (peaks) and local minima (troughs). To better suit our specific application, we modify the second step of this algorithm, in which the turning point list is refined. Full details are included in Appendix A. We display 12 countries' mortality rate time series and annotate their turning points in Figure 1.

To quantify distance between time series' turning points, we modify the semi-metric of [39] (with $p = 1$). Given two non-empty finite sets $S_1, S_2 \subset \{1, 2, \dots, T\}$, this is defined as

$$D(S_1, S_2) = \frac{1}{2T} \left(\frac{\sum_{b \in S_2} d(b, S_1)}{\#S_2} + \frac{\sum_{a \in S_1} d(a, S_2)}{\#S_1} \right), \quad (2)$$

where $d(b, S_1)$ is the minimal distance from $b \in S_2$ to the set S_1 , and $\#S_1$ is the cardinality of S_1 , and analogously for S_2 . By the choice of normalisation, this is always bounded between 0 and 1. To more appropriately separate different behaviours among mortality trends, we modify this semi-metric by including a regularisation term as follows:

$$D'(S_1, S_2) = D(S_1, S_2) + \beta |\#S_1 - \#S_2|, \quad (3)$$

where $0 < \beta < 1$ is a constant. The resulting values $D'(S_1, S_2)$ are symmetric, non-negative, and zero if and only if $S_1 = S_2$. Then, we define the $n \times n$ matrix

D^{TP} between turning point sets by

$$D_{ij}^{TP} = D'(P_i, P_j) + D'(T_i, T_j). \quad (4)$$

We perform hierarchical clustering on D^{TP} in Figure 2, with $\beta = 1/3$ (as a compromise between the usual sizes of $D(S_1, S_2)$ and $|\#S_1 - \#S_2|$). These distances do not capture the absolute values of the mortality rate time series; they only distinguish between their undulating behaviour, reflected in their sets of turning points. To round out our analysis, we include another metric, an L^1 norm that does account for difference in the absolute values of mortality. We define another matrix by

$$D_{ij}^1 = \sum_{t=30}^T |r_i(t) - r_j(t)|, \quad (5)$$

and perform hierarchical clustering on D^1 in Figure 3.

2.2. Results

In Figure 1, we display rolling mortality rate and turning points for 12 countries: Brazil, India, Mexico, the United States (US), the Netherlands, Sweden, France, Germany, Italy, Russia, Ecuador and Bulgaria. These countries display highly heterogeneous behaviours, which are suitably captured in Figure 2. This dendrogram reveals four clusters of similarity, and one outlier. Russia (1j) is the unique country with just two detected turning points. Several developing countries such as Brazil (1a), India (1b) and Mexico (1c) as well as developed countries including the US (1d), the Netherlands (1e) and Sweden (1f) have three turning points. France (1g), Germany (1h) and Italy (1i) have four turning points. Ecuador (1k) and others have five, while Bulgaria (1l) and others have six.

Within the 4-turning point cluster, we see a dense subcluster of similarity containing Austria, Belgium, Canada, Czechia, France, Georgia, Germany, Hungary, Italy, Poland, Portugal, Switzerland and the United Kingdom (UK). All these countries experienced a peak in the mortality rate in April or May (corresponding to the previous 30 days) and a local minimum near the beginning of September (corresponding to the previous 30 days during August). This similarity can be seen by examining members of this cluster, France (1g), Germany (1h) and Italy (1i).

Turning to Figure 3, several other insights concerning the mortality rate trajectories emerge. First, Mexico and Ecuador are identified as outliers in the collection of countries, with only slight similarity to each other. For Mexico (1c), this is due to a consistently high mortality rate over time, over 10% for most of the period. Ecuador (1k) is an outlier due to peaks in mortality over 30%, higher than any other country. Belgium, France, Hungary, Spain, and the UK form their own smaller cluster characterised by high mortality rates (of around 20%) in their first wave of COVID-19. Indeed, these countries experienced higher mortality in March-April than anywhere else in the world.

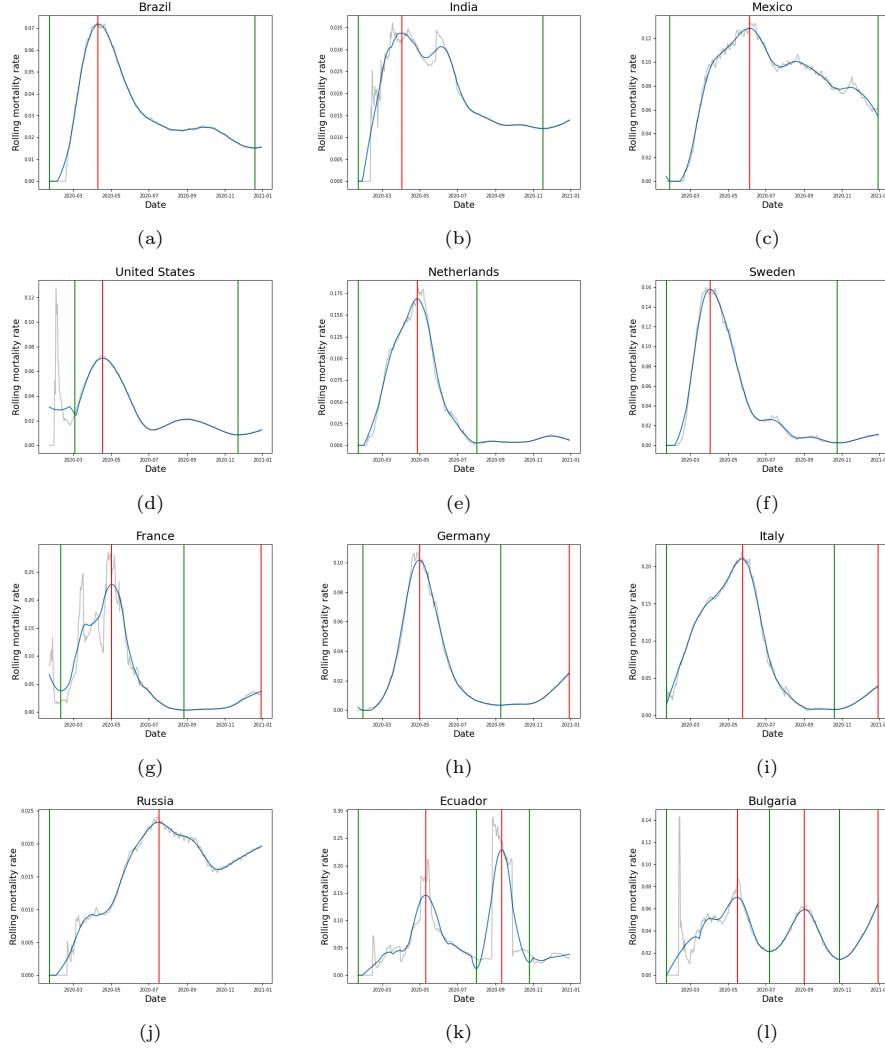


Figure 1: Smoothed mortality rate time series and identified turning points for various countries: (a) Brazil (b) India (c) Mexico (d) the US (e) the Netherlands (f) Sweden (g) France (h) Germany (i) Italy (j) Russia (k) Ecuador (l) Bulgaria. Green and red vertical lines denote algorithmically detected troughs and peaks, respectively. The rolling mortality rate at a given time calculates the mortality over the previous 30 days. The aforementioned countries represent at least one member of every characteristic class of trajectories.

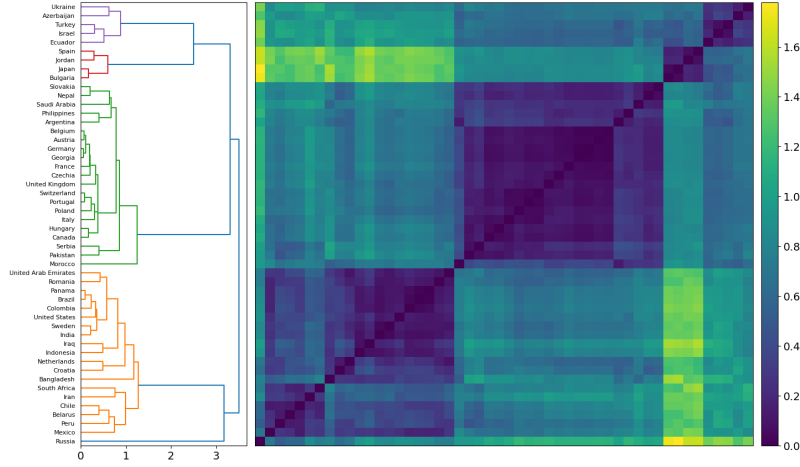


Figure 2: Hierarchical clustering on the turning point distance matrix D^{TP} , defined in Section 2. This groups countries according to their similarity in undulating behaviour, measured by distances between turning point sets. Five characteristic classes are observed: Russia has two turning points; Brazil, India and the US have three; most European countries have four, with a strong subcluster of similarity observed including Austria, Belgium, and others. Two smaller classes are observed containing five and six turning points, respectively.

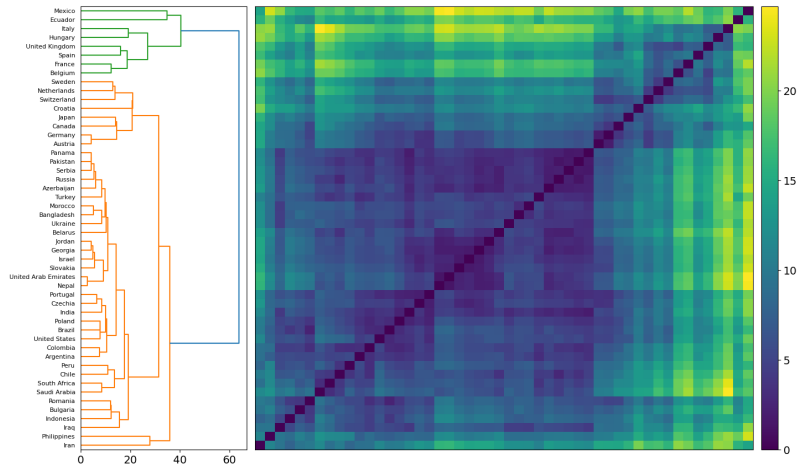


Figure 3: Hierarchical clustering on the L^1 distance matrix D^1 , defined in Section 2. Mexico and Ecuador emerge as outliers, characterised by a consistently high mortality rate over the full period and the highest peaks in mortality of all, respectively. Belgium, France, Hungary, Spain and the UK are revealed as a secondary cluster, characterised by high mortality in April and May, rapidly decreasing from then.

3. Virulence matrix analysis

In this section, we develop a new framework of time-varying analysis of 30-day rolling *virulence matrices*, inspired by, but differing from, covariance matrices in finance [40]. Let $t = 30, \dots, T$ be a particular time. We form vectors $\mathbf{x}_i(t) = (x_i(t-29), \dots, x_i(t))$, analogously for $\mathbf{y}_i(t)$. These two vectors record the case and death counts over the past 30 days. We may also form $\mathbf{r}_i(t) = (r_i(t-29), \dots, r_i(t))$ for $t = 59, \dots, T$, as the time series $r_i(t)$ only begin at $t = 30$. Define (unscaled) inner products by

$$\langle \mathbf{x}_i(t), \mathbf{x}_j(t) \rangle = \sum_{s=t-29}^t x_i(s)x_j(s). \quad (6)$$

We then define $n \times n$ (unscaled) virulence matrices with respect to cases, deaths and mortality rates by the following ($i, j = 1, \dots, n$):

$$V_{ij}^c(t) = \langle \mathbf{x}_i(t), \mathbf{x}_j(t) \rangle, t = 30, \dots, T; \quad (7)$$

$$V_{ij}^d(t) = \langle \mathbf{y}_i(t), \mathbf{y}_j(t) \rangle, t = 30, \dots, T; \quad (8)$$

$$V_{ij}^r(t) = \langle \mathbf{r}_i(t), \mathbf{r}_j(t) \rangle, t = 59, \dots, T. \quad (9)$$

We could also analogously define normalised virulence matrices by using normalised inner products in place of the unscaled inner products above. These matrices are thus named because they provide a representation of the global spread of COVID-19 over the last 30 days and contain relationships between different countries' trajectories. The use of a standard covariance matrix here would not appropriately measure this prevalence: a country with a constant (but severe) number of cases for the past 30 days would yield a zero covariance with any other country. Each matrix $V(t)$ is a $n \times n$ symmetric real matrix, and thus is diagonalisable with all real eigenvalues. By the positivity of the inner product, each matrix satisfies a non-negativity condition $\mathbf{u}^T V \mathbf{u} \geq 0$ for $\mathbf{u} \in \mathbb{R}^n$, and so all eigenvalues are non-negative. We list and order the eigenvalues $\lambda_1 \geq \lambda_2 \geq \dots \geq \lambda_n \geq 0$. This produces a time-varying eigenspectrum, which we display in Figure 4 for the first ten eigenvalues. Moreover, for any such symmetric matrix, the greatest eigenvalue λ_1 holds particular significance. By the spectral theorem, λ_1 coincides with the *operator norm* of the matrix [41], a measure of its total size. That is,

$$\lambda_1 = \|V\|_{op} = \max_{\mathbf{u} \in \mathbb{R}^n - \{0\}} \frac{\|V\mathbf{u}\|}{\|\mathbf{u}\|}. \quad (10)$$

Subsequent eigenvalues also have a real-world interpretation. $\lambda_2 = 0$ if and only if the matrix V is rank 1, which occurs if and only if all trajectories \mathbf{x}_i (in the instance of the cases matrix) differ by a multiplicative constant. In general, a small value of λ_2 relative to λ_1 indicates substantial homogeneity in the trajectories.

In Figures 4a, 4b and 4c, respectively, we display the time-varying eigenspectra

for the virulence matrices associated to cases, deaths and mortality rates. There are several interesting properties of these time-varying eigenspectra. The first eigenvalue λ_1 of Figure 4a demonstrates the general increase of new COVID-19 cases over the course of 2020. The sharp spike towards the end of the year demonstrates the rapid growth in cases in the final months of 2020. Figure 4b has two prominent peaks in its first eigenvalue, corresponding to the periods of March-April and November-December. These peaks highlight the natural history of COVID-19, where many countries suffered significant deaths during their first wave of the virus, enforced harsh restrictions resulting in fewer cases and deaths, and subsequently experienced further growth in cases and deaths upon such restrictions' easing. Finally, the first eigenvalue in Figure 4c highlights an interesting trend in the mortality rate. There is a marked spike in March-April, followed by a significant reduction throughout the remainder of 2020. This shape in the first eigenvalue likely represents vulnerable people dying earlier and/or under-reporting of cases early in the year, contributing to a higher calculated mortality rate from reported cases and deaths.

The relationship between the first eigenvalue and subsequent eigenvalues is also of interest. Figure 4a shows the second eigenvalue λ_2 becoming quite significant for cases towards the end of 2020, when the total number of cases is larger than ever. This shows that the behaviour of new cases in late 2020 is more heterogeneous than the first wave, when all cases were rising quite uniformly throughout the world. Figures 4b and 4c show a more moderate, but similar phenomenon concerning deaths and mortality rate at various stages of the year. The second eigenvalue in Figure 4b is slightly more pronounced in the second wave of the virus, displaying more heterogeneity in COVID-19 deaths later in the year. The second eigenvalue in Figure 4c is more pronounced during the first wave of the virus - highlighting more heterogeneity during the first wave of the virus with respect to mortality. Indeed, Figure 1 shows that European countries experienced substantial mortality in their first wave of COVID-19, which characterised them as anomalous in Figure 3. This contributed to a meaningful heterogeneity of mortality rates across the world during the early stages of the year.

4. Inconsistency analysis

In this section, we describe how we measure the consistency between three attributes, and reveal anomalous countries in the process. To do so, we introduce a new method of comparing three distance matrices and apply this to distances between case and death time series, and human development indices (HDI). Let h_i be the HDI of each country. Calculated by the United Nations Development Programme [42], this index combines a country's life expectancy, educational standards and economic standard of living. Bounded between 0 and 1, the HDI h_i reflects a substantially lower living standard the further h moves from 1. To reflect this, we use a logarithmic distance between these indices that penalises

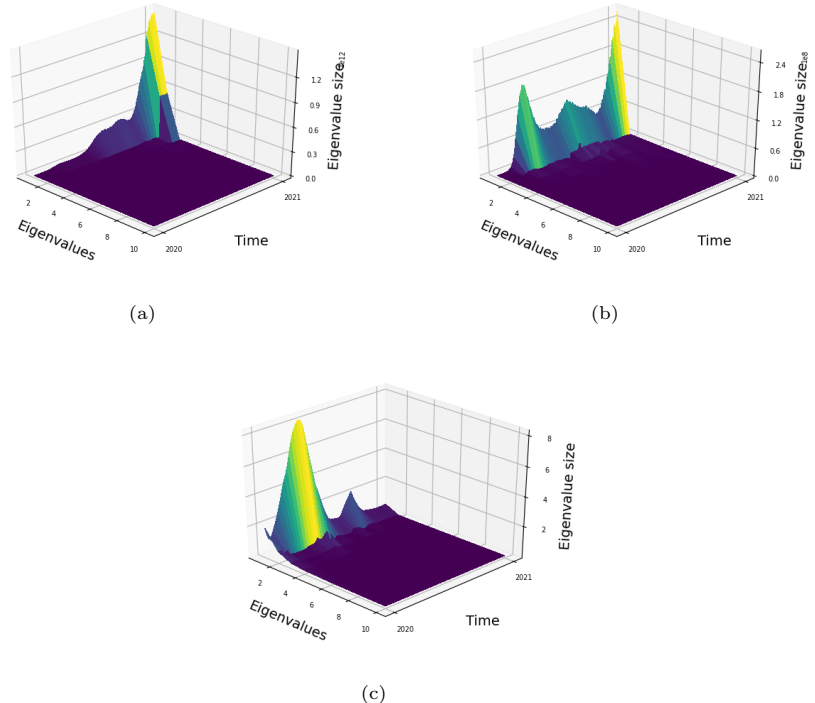


Figure 4: Time-varying eigenspectra (first ten eigenvalues) for the virulence matrices associated to (a) cases (b) deaths (c) mortality rate. The first eigenvalue demonstrates broad trends in the total size of the matrices, and shows (a) a large increase of cases towards the end of 2020, (b) two or three waves of significant deaths, (c) the highest mortality early on in the year. The second eigenvalue reveals more heterogeneity in case trajectories towards the end of the year, and mortality towards the beginning of the year.

movement away from 1 more than a linear distance:

$$D_{ij}^h = |\log h_i - \log h_j|, i, j = 1, \dots, n. \quad (11)$$

This forms a $n \times n$ distance matrix between countries' development indices. Given the exponential nature of the spread of the virus, we also use a logarithmic distance between the case and death time series. Some of these time series have negative counts due to retrospective adjustments in the data. In order to ensure non-negative counts, we first apply a Savitzky-Golay filter to produce smoothed case and death time series $\hat{x}_i(t)$ and $\hat{y}_i(t)$ respectively. Due to its moving average and polynomial smoothing, this eliminates almost all negatives, except when there are very few counts. We replace any non-positive count with a 1. Then, we may calculate a logarithmic L^1 distance as follows:

$$D_{ij}^c = \|\log \hat{x}_i - \log \hat{x}_j\| = \sum_{t=1}^T |\log \hat{x}_i(t) - \log \hat{x}_j(t)|; \quad (12)$$

$$D_{ij}^d = \|\log \hat{y}_i - \log \hat{y}_j\| = \sum_{t=1}^T |\log \hat{y}_i(t) - \log \hat{y}_j(t)|. \quad (13)$$

We use such a metric between case or death time series rather than a simple difference between the total yearly counts to distinguish between countries (and hence reveal potential anomalies) according to when the cases or deaths occurred. Thus, we have defined three $n \times n$ distance matrices between countries. Given a $n \times n$ distance matrix D , its corresponding *affinity matrix* is defined as

$$A_{ij} = 1 - \frac{D_{ij}}{\max \{D\}}, i, j = 1, \dots, n. \quad (14)$$

All elements of these affinity matrices lie in $[0, 1]$, so it is appropriate to compare them directly by taking their difference. Given a $n \times n$ matrix C , let $|C|$ be the matrix given by taking the absolute value of all elements, that is $|C|_{ij} = |C_{ij}|$. Then, define three $n \times n$ symmetric pairwise inconsistency matrices:

$$\text{INC}^{c,d} = |A^c - A^d|; \quad (15)$$

$$\text{INC}^{c,h} = |A^c - A^h|; \quad (16)$$

$$\text{INC}^{d,h} = |A^d - A^h|; \quad (17)$$

and a total inconsistency matrix

$$\text{INC}^{c,d,h} = \text{INC}^{c,d} + \text{INC}^{c,h} + \text{INC}^{d,h}. \quad (18)$$

Next, we can define pairwise anomaly scores by

$$a_i^{c,d} = \sum_{j=1}^n \text{INC}_{ij}^{c,d}; \quad (19)$$

$$a_i^{c,h} = \sum_{j=1}^n \text{INC}_{ij}^{c,h}; \quad (20)$$

$$a_i^{d,h} = \sum_{j=1}^n \text{INC}_{ij}^{d,h}. \quad (21)$$

For each country, we record an *anomaly vector* $\mathbf{a}_i = (a_i^{c,d}, a_i^{c,h}, a_i^{d,h})$ and a *total anomaly score* given by $a_i^{c,d,h} = a_i^{c,d} + a_i^{c,h} + a_i^{d,h}$. We can also define a *weighted anomaly score* to reduce bias in one set of anomaly scores being systematically larger than another. Let $M^{c,d} = \max_i \{a_i^{c,d}\}$, analogously for $M^{c,h}$ and $M^{d,h}$. Let the weighted anomaly score be $\tilde{a}_i^{c,d,h} = a_i^{c,d}/M^{c,d} + a_i^{c,h}/M^{c,h} + a_i^{d,h}/M^{d,h}$. This aims to record a neutral contribution from each anomaly score. In Tables 1 and 2, we record the anomaly vectors, total anomaly score and weighted anomaly score for all 50 countries under consideration. In Figure 5, we plot the total consistency matrix $\text{INC}^{c,d,h}$, where anomalous countries can easily be seen due to larger entries in their respective rows and columns. An analogous weighted consistency matrix can also be defined, which is broadly similar to the one shown.

The total inconsistency matrix and all computed anomaly scores yield several insights. First, the three most anomalous countries with respect to the weighted anomaly score are Pakistan, the US and the United Arab Emirates (UAE). A near-identical result applies if we use the unscaled total anomaly score, with Pakistan, the US, Nepal and then the UAE exhibiting the largest unscaled scores. For the US and Pakistan, the highest contribution to the total or weighted anomaly score comes from their high pairwise anomaly scores $a^{c,h}$ and $a^{d,h}$, which are the two highest of any country. Interestingly, these high scores have differing explanations. The US is highly inconsistent between cases (and analogously deaths) and HDI due to its much higher case and death counts than other countries of similar HDI. Pakistan is classified as inconsistent due to an extreme HDI, the lowest of any country under consideration, but a case and death time series that are similar to many others. Thus, due to a lower HDI than other countries with similar case and death counts, it is registered as inconsistent. We remark that high anomaly scores do not necessarily indicate a straight-forward anomalous quotient between cases or HDI, for example. Instead, a high anomaly score reflects inconsistency in relationships with other countries.

On the other hand, the UAE has a high weighted and total anomaly score due to its value of $a^{c,d}$, which is the highest of any country. Indeed, the UAE experienced the lowest mortality rate across 2020 of any country under consideration. The country with the second-highest value of $a^{c,d}$ is Mexico. This is anomalous for the opposite reason: a consistently high progression from cases

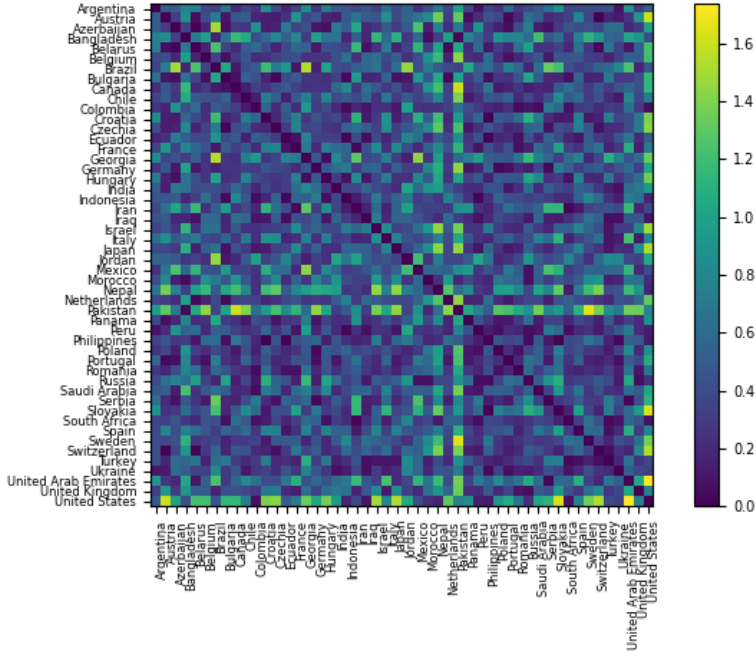


Figure 5: Total anomaly matrix $\text{INC}^{c,d,h}$, as defined in Section 4. Lighter entries indicate higher values of the matrix, and hence more inconsistency between the attributes under consideration: cases, deaths and HDI. The US and Pakistan can be seen to have substantial inconsistency with many other countries.

to deaths, as first noted in Figure 1c.

5. Discussion and conclusion

In this paper, we analyse the natural history of COVID-19 across 50 countries over 2020. We observe significant structural similarity between certain countries as well as heterogeneity across the world with respect to COVID-19 prevalence and mortality, and identify anomalous countries therein.

In Section 2, we analyse mortality rate trajectories for 50 countries. By modifying a recently introduced turning point algorithm and introducing a new semi-metric between turning point sets, we assign these time series into five characteristic classes according to their differing trajectories. Russia is identified as an outlier - its mortality rate rose consistently until July and never dropped substantially enough to register a subsequent trough in our algorithmic framework. It is unique in this sense among the 50 countries, possessing a consistently stable mortality rate after its first peak. 19 countries exhibit three turning points, including Brazil, India and the US, indicating a substantial

Country anomaly scores relative to cases, deaths and HDI (1)					
Country	$a^{c,d}$	$a^{c,h}$	$a^{d,h}$	$a^{c,d,h}$	$\tilde{a}^{c,d,h}$
Argentina	3.23	8.96	10.59	22.78	1.98
Austria	3.43	8.73	10.45	22.61	1.20
Azerbaijan	3.87	7.47	9.72	21.06	1.15
Bangladesh	2.47	14.69	14.93	32.10	1.58
Belarus	4.41	7.86	9.91	22.19	1.23
Belgium	3.88	8.27	8.52	20.67	1.13
Brazil	4.04	12.29	15.31	31.64	1.64
Bulgaria	2.26	8.84	8.31	19.41	0.99
Canada	2.87	9.15	9.21	21.23	1.11
Chile	3.00	9.18	10.85	23.04	1.20
Colombia	3.55	6.28	6.48	16.30	0.92
Croatia	2.91	10.53	11.04	24.48	1.26
Czechia	4.06	8.23	9.86	22.15	1.21
Ecuador	3.75	7.52	6.96	18.23	1.02
France	2.98	9.77	10.70	23.45	1.21
Georgia	4.86	13.33	11.92	30.11	1.61
Germany	3.33	9.83	8.36	20.62	1.10
Hungary	3.52	10.74	8.94	23.21	1.23
India	2.75	9.67	9.72	22.14	1.14
Indonesia	3.72	8.37	7.47	19.56	1.07
Iran	5.25	8.77	11.68	25.69	1.43
Iraq	3.42	7.35	5.88	16.65	0.93
Israel	4.98	9.74	11.15	25.86	1.43
Italy	4.03	9.27	11.67	24.96	1.34
Japan	2.79	9.75	10.34	22.88	1.18
Jordan	4.66	11.06	10.94	26.66	1.44
Mexico	9.73	6.82	13.06	29.60	1.85
Morocco	3.97	10.34	9.67	24.00	1.29
Nepal	4.53	16.84	17.78	39.15	2.00
Netherlands	3.97	8.41	8.70	21.08	1.16
Pakistan	2.43	22.73	21.65	46.80	2.24
Panama	3.34	7.17	7.92	18.42	1.01
Peru	3.06	6.48	6.98	16.52	0.90
Philippines	2.51	7.49	7.29	17.29	0.91
Poland	2.68	7.69	8.58	18.94	0.99
Portugal	3.11	7.42	8.10	18.63	1.00
Romania	3.18	7.24	7.68	18.10	0.98

Table 1: Anomaly vectors, total anomaly scores and weighted anomaly scores, as defined in Section 4, for the first 37 countries under consideration. Pairwise anomaly scores quantify the inconsistency in measurements between two quantities, while the total and weighted anomaly scores incorporate all three attributes. The weighted anomaly score is chosen to more appropriately weight the contributions from the three pairwise scores.

Country anomaly scores relative to cases, deaths and HDI (2)					
Country	$a^{c,d}$	$a^{c,h}$	$a^{d,h}$	$a^{c,d,h}$	$\tilde{a}^{c,d,h}$
Russia	2.62	10.62	10.75	23.99	1.21
Saudi Arabia	3.10	10.77	10.54	24.41	1.26
Serbia	3.57	7.98	9.80	21.36	1.15
Slovakia	3.34	12.86	13.13	29.33	1.50
South Africa	3.16	7.01	5.72	15.89	0.88
Spain	4.05	9.82	11.27	25.14	1.35
Sweden	4.23	9.57	9.36	23.16	1.26
Switzerland	3.14	8.52	9.73	21.38	1.13
Turkey	2.50	7.81	7.78	18.08	0.95
Ukraine	2.78	6.86	6.45	16.08	0.87
UAE	10.29	8.78	13.56	32.63	2.01
UK	3.78	9.87	10.80	24.44	1.30
US	3.18	18.46	19.81	41.45	2.04

Table 2: Anomaly vectors, total anomaly scores and weighted anomaly scores, as defined in Section 4, for the remaining 13 countries under consideration. Pairwise anomaly scores quantify the inconsistency in measurements between two quantities, while the total and weighted anomaly scores incorporate all three attributes. The weighted anomaly score is chosen to more appropriately weight the contributions from the three pairwise scores.

reduction in mortality from a first peak. 21 countries exhibit four turning points, indicating a second wave in which mortality has increased once again. In particular, a strong subcluster contains most Western European countries: Austria, Belgium, Czechia, France (1g), Germany (1h), Hungary, Italy (1i), Portugal, Switzerland, and the UK. These all share highly similar mortality trajectories, with a first peak in April-May, a trough around September, and another peak at the end of the year.

There are three wealthy western European countries that do not fit into this cluster. Both the Netherlands and Sweden, displayed in Figures 1e and 1f respectively, do not register a second peak in mortality. Indeed, these countries both kept their mortality low towards the end of the year, while France, Germany and Italy experienced an increase. Prior research has noted that the Netherlands reduced its mortality rate substantially in its second wave of COVID-19 [43], while Sweden changed its COVID-19 response substantially relative to the first half of the year [44]. Spain registers six turning points primarily due to highly irregular reporting, featuring negative counts and large numbers of cases and deaths consolidated and reported on single sporadic days.

A smaller number of countries exhibited more turning points: five with 5 turning points and four with 6. We observe that the majority of developed countries exhibit 3 or 4 turning points, as visible in Figure 2, while the outlier countries (with 2,5 or 6 turning points) were mostly developing countries. This reflects more regular (and less undulating) behaviour in the mortality rate trajectories and has two explanations. First, more developed countries may have implemented more consistent testing, which could have caused less fluctuations

in the reported mortality rate. Secondly, more developed countries may have more healthcare resources to improve their treatment of COVID-19 and thereby reduce and stabilise the mortality rate over time.

In Section 3, we introduce a new class of virulence matrices for cases, deaths and mortality rates and analyse their eigenspectra. The first eigenvalue λ_1 provides a measure of the total scale of the matrices and summarises worldwide trends in prevalence and mortality throughout 2020. Figure 4a reflects a substantial surge in cases towards the end of the year, Figure 4b shows multiple waves of deaths of comparable magnitude, while Figure 4c shows an early peak that dominates the rest of the period. The second eigenvalue λ_2 provides a measure of the heterogeneity among the studied time series. Figure 4a exhibits a considerable rise in heterogeneity towards the end of the year, during a time in which new cases trajectories across different countries were substantial but quite non-uniform. In Figure 4b, we see a much greater value of λ_2 during the second wave of deaths, in which λ_1 is in fact lower than the first wave. The much milder drop off between λ_1 and λ_2 indicates the greatest heterogeneity with respect to deaths during this period in the middle of the year. Figure 4c similarly reveals substantial heterogeneity in mortality rates during the earlier part of the year.

When viewed in conjunction, these three figures provide several insights into the natural history of the disease throughout 2020. Case counts generally increased in global severity throughout the year, while death counts constituted a much clearer pattern of multiple waves. The mortality rate trajectory (4c) can explain this - in March and April, the progression from reported cases to deaths was much more severe throughout Europe, causing substantial deaths despite fewer cases than late 2020. During the middle of the year, the heterogeneity in death counts was at its highest. Indeed, the months of June to August featured relatively few new cases in Europe [45], while Brazil [46], India and other developing countries experienced substantial growth in cases [47]. Towards the end of the year, the pandemic once again impacted the entire world, with more counts observed than ever before. During this time, mortality was low, but cases were so high that deaths became the highest they have ever been. Heterogeneity in case trajectories also increased substantially, with COVID-19 trajectories differing substantially between different countries, many increasing, some decreasing, but most with high total counts. One could more closely examine heterogeneity by considering normalised virulence matrices obtained from normalised inner products, as explained in Section 3.

In Section 4, we study the consistency between cases, deaths and HDI for all 50 countries under consideration. We believe that this is the first method proposed to study (in)consistencies among a collection of time series for up to three measures. We propose two measures of anomaly across these three quantities: a total and weighted anomaly score (that more appropriately combines the contributions of the three pairwise anomaly components). The three most anomalous countries with respect to the weighted score are Pakistan, the US and the UAE. Closer inspection of the pairwise anomaly components in Tables 1 and 2 can reveal which quantities most contribute to a country's total or weighted score. For the UAE, this is the high anomaly score between cases and deaths,

caused by the lowest progression from cases to deaths among our collection of countries. For the US, both anomaly scores $a^{c,h}$ and $a^{d,h}$ contribute highly; these reflect the fact that the US has considerably more cases and deaths than other countries of similar HDI. For Pakistan, the same two anomaly scores $a^{c,h}$ and $a^{d,h}$ are the largest of any country, but for the opposite reason: its HDI is substantially lower than any country with a similar case and death time series.

The full collection of anomaly scores can also reveal broad trends regarding consistency between the three measures. In Tables 1 and 2, we see that the two pairwise anomaly scores relative to HDI are systematically greater than the pairwise score between case and death counts. Indeed, we have $a_i^{c,d} < a_i^{d,h}$ for every single country and $a_i^{c,d} < a_i^{c,h}$ for every country except Mexico (which has the second-highest case-death anomaly score after the UAE due to its consistently and anomalously high mortality). These patterns reveal systematically more consistency between case and death counts than between case or death counts and HDI. Qualitatively, this reveals there is little relationship between a country's HDI and its case or death counts. In addition, a closer examination reveals that $a_i^{c,h} < a_i^{d,h}$ for 34 out of the 50 countries, 2/3 of the collection. Thus, to a lesser extent, there is greater consistency between case counts and HDI than there is between death counts and HDI. This is a surprising finding - one would naively expect more consistency between a lower HDI and higher deaths due to poorer healthcare quality resulting in a greater progression of cases to deaths, regardless of the number of cases.

Several limitations and opportunities for future research exist in this inconsistency framework. First, the results could also be repeated for case and death time series as a proportion of each country's population. Alternative metrics between cases and deaths could be used, such as a simple difference between the total yearly counts, without the temporal component provided by the L^1 metric. A closer analysis of the relationship between the varying sizes of the anomaly scores could quantitatively characterise the differing consistency between three quantities as a whole. One limitation in this analysis framework is that anomalies are measured purely by their relative deviation from the rest of the collection, and direction (positive or negative) is ignored. A closer inspection is necessary to determine the nature of the anomaly. However, this could be seen as a benefit of the methodology as well, as it is flexible in the detection of different sorts of inconsistent behaviour.

Overall, this paper introduces new methods for analysing COVID-19 prevalence and mortality on a country-by-country and worldwide basis and chronicles the natural history of COVID-19 during 2020. On a global scale, we reveal broad trends in case and death counts as well as mortality trajectories, which present a coherent picture of the changing impacts of COVID-19 over time. On a country-by-country basis, we reveal both heterogeneity and structural similarity with respect to mortality over time and study consistency between COVID-19 prevalence and human development, revealing specific anomalous countries. Moreover, the framework presented in this paper could be applied broadly to various epidemiological or economic crises.

As 2021 begins, the world remains severely affected by COVID-19. Though vaccination distribution is underway in many countries, the analysis of trends in cases, deaths and mortality remains of substantial relevance to governments. The identification of structural similarity in mortality rate trajectories between European states may inspire additional cooperation [7] and coordination of their strategic response to the pandemic. Our methods highlight countries that have responded particularly well or poorly, and our analysis highlights points in time where cases, deaths and mortality rates changed substantially for candidate countries. Finally, we reveal global changes in the relationship between cases, deaths and mortality rates over time. Such changes should inform governments regarding their response to the pandemic. This will be particularly crucial in the coming months, as various vaccines are administered over the world.

Data availability

Daily COVID-19 case and death counts and human development index data can be accessed at "Our World in Data" [48].

Appendix A. Turning point methodology

In this section, we provide more details for the identification of turning points of a mortality rate time series $r(t)$. First, some smoothing is necessary due to irregularities in the data set, and discrepancies between different data sources. The Savitzky-Golay filter ameliorates these issues by combining polynomial smoothing with a moving average computation, and yields a smoothed time series $\hat{r}(t) \in \mathbb{R}_{\geq 0}$. Subsequently, we perform a two-step process to select and then refine a non-empty set P of local maxima (peaks) and T of local minima (troughs).

Following [15], we apply a two-step algorithm to the smoothed time series $\hat{r}(t)$. The first step produces an alternating sequence of troughs and peaks. The second step refines this sequence according to chosen conditions and parameters. The most important conditions to identify a peak or trough, respectively, in the first step, are the following:

$$\hat{r}(t_0) = \max\{\hat{r}(t) : \max(1, t_0 - l) \leq t \leq \min(t_0 + l, T)\}, \quad (\text{A.1})$$

$$\hat{r}(t_0) = \min\{\hat{r}(t) : \max(1, t_0 - l) \leq t \leq \min(t_0 + l, T)\}, \quad (\text{A.2})$$

where l is a parameter to be chosen. Following [15], we select $l = 17$, which accounts for the 14-day incubation period of the virus [49] and less testing on weekends. Defining peaks and troughs according to this definition alone has several flaws, such as the potential for two consecutive peaks.

Instead, we implement an inductive procedure to choose an alternating sequence of peaks and troughs. Suppose t_0 is the last determined peak. We search in the period $t > t_0$ for the first of two cases: if we find a time $t_1 > t_0$ that satisfies (A.2) as well as a non-triviality condition $\hat{r}(t_1) < \hat{r}(t_0)$, we add

t_1 to the set of troughs and proceed from there. If we find a time $t_1 > t_0$ that satisfies (A.1) and $\hat{r}(t_0) \geq \hat{r}(t_1)$, we ignore this lower peak as redundant; if we find a time $t_1 > t_0$ that satisfies (A.1) and $\hat{r}(t_1) > \hat{r}(t_0)$, we remove the peak t_0 , replace it with t_1 and continue from t_1 . A similar process applies from a trough at t_0 .

At this point, the time series is assigned an alternating sequence of troughs and peaks. However, some turning points are immaterial and should be excluded. The second step is a flexible approach introduced in [15] for this purpose. In this paper, we introduce new conditions within this framework. First, we use the same peak ratio procedure: let $t_1 < t_3$ be two peaks, necessarily separated by a trough. We select a parameter $\delta = 0.2$, and if the *peak ratio*, defined as $\frac{\hat{r}(t_3)}{\hat{r}(t_1)} < \delta$, we remove the peak t_3 . If two consecutive troughs t_2, t_4 remain, we remove t_2 if $\hat{r}(t_2) > \hat{r}(t_4)$, otherwise remove t_4 . That is, if the second peak has size less than δ of the first peak, we remove it.

Finally, let t_1, t_2 be adjacent turning points (one a trough, one a peak). We choose a parameter $\epsilon = \log(2)$; if

$$|\log \hat{r}(t_2) - \log \hat{r}(t_1)| < \epsilon, \quad (\text{A.3})$$

that is, the values of the turning point differ by less than a factor of 2, we remove t_2 from our sets of peaks and troughs. If t_2 is not the final turning point, we also remove t_1 . This is a different condition from previous work - whereas [15] considers the average change with time between turning points of new case trajectories, we consider only the absolute change between turning points in mortality rate. Indeed, there is no need to consider how much time has passed when determining whether mortality has increased or decreased by a sufficient amount, in our implementation a factor of 2, to warrant a turning point being included.

References

- [1] M. Wang, et al., Remdesivir and chloroquine effectively inhibit the recently emerged novel coronavirus (2019-nCoV) in vitro, *Cell Research* 30 (2020) 269–271. doi:10.1038/s41422-020-0282-0.
- [2] E. M. Bloch, Convalescent plasma to treat COVID-19, *Blood* 136 (2020) 654–655. doi:10.1182/blood.2020007714.
- [3] X. Xu, et al., Effective treatment of severe COVID-19 patients with tocilizumab, *Proceedings of the National Academy of Sciences* 117 (2020) 10970–10975. doi:10.1073/pnas.2005615117.
- [4] B. Cao, et al., A trial of Lopinavir-Ritonavir in adults hospitalized with severe Covid-19, *New England Journal of Medicine* 382 (2020) 1787–1799. doi:10.1056/nejmoa2001282.

- [5] F. P. Polack, et al., Safety and efficacy of the BNT162b2 mRNA Covid-19 vaccine, *New England Journal of Medicine* 383 (2020) 2603–2615. doi:10.1056/nejmoa2034577.
- [6] E. E. Walsh, et al., Safety and immunogenicity of two RNA-based Covid-19 vaccine candidates, *New England Journal of Medicine* 383 (2020) 2439–2450. doi:10.1056/nejmoa2027906.
- [7] V. Priesemann, et al., Calling for pan-European commitment for rapid and sustained reduction in SARS-CoV-2 infections, *The Lancet* 397 (2021) 92–93. doi:10.1016/s0140-6736(20)32625-8.
- [8] S. Momtazmanesh, et al., All together to fight COVID-19, *The American Journal of Tropical Medicine and Hygiene* 102 (2020) 1181–1183. doi:10.4269/ajtmh.20-0281.
- [9] S. McDonell, Coronavirus: US and Australia close borders to Chinese arrivals, <https://www.bbc.com/news/world-51338899>, 2020. BBC, February 2, 2020.
- [10] J. McCurry, Test, trace, contain: how South Korea flattened its coronavirus curve, <https://www.theguardian.com/world/2020/apr/23/test-trace-contain-how-south-korea-flattened-its-coronavirus-curve>, 2020. The Guardian, U.S. April 23, 2020.
- [11] A. McCann, N. Popovich, J. Wu, Italy's virus shutdown came too late. what happens now?, <https://www.nytimes.com/interactive/2020/04/05/world/europe/italy-coronavirus-lockdown-reopen.html>, 2020. The New York Times, April 5, 2020.
- [12] G. Scally, B. Jacobson, K. Abbasi, The UK's public health response to covid-19, *BMJ* (2020) m1932. doi:10.1136/bmj.m1932.
- [13] M. Iati, et al., All 50 U.S. states have taken steps toward reopening in time for Memorial Day weekend, <https://www.washingtonpost.com/nation/2020/05/19/coronavirus-update-us>, 2020. The Washington Post, May 20, 2020.
- [14] R. Meyer, A. C. Madrigal, A devastating new stage of the pandemic, <https://www.theatlantic.com/science/archive/2020/06/second-coronavirus-surge-here/613522>, 2020. The Atlantic, June 25, 2020.
- [15] N. James, M. Menzies, COVID-19 in the United States: Trajectories and second surge behavior, *Chaos: An Interdisciplinary Journal of Nonlinear Science* 30 (2020) 091102. doi:10.1063/5.0024204.
- [16] S. Funk, A. Camacho, A. J. Kucharski, R. M. Eggo, W. J. Edmunds, Real-time forecasting of infectious disease dynamics with a stochastic semi-mechanistic model, *Epidemics* 22 (2018) 56–61. doi:10.1016/j.epidem.2016.11.003.

- [17] A. Mhlanga, Dynamical analysis and control strategies in modelling ebola virus disease, *Advances in Difference Equations* 2019 (2019). doi:10.1186/s13662-019-2392-x.
- [18] S. K. Biswas, U. Ghosh, S. Sarkar, Mathematical model of Zika virus dynamics with vector control and sensitivity analysis, *Infectious Disease Modelling* 5 (2020) 23–41. doi:10.1016/j.idm.2019.12.001.
- [19] R. E. Morrison, A. Cunha, Embedded model discrepancy: A case study of Zika modeling, *Chaos: An Interdisciplinary Journal of Nonlinear Science* 30 (2020) 051103. doi:10.1063/5.0005204.
- [20] C. Manchein, E. L. Brugnago, R. M. da Silva, C. F. O. Mendes, M. W. Beims, Strong correlations between power-law growth of COVID-19 in four continents and the inefficiency of soft quarantine strategies, *Chaos: An Interdisciplinary Journal of Nonlinear Science* 30 (2020) 041102. doi:10.1063/5.0009454.
- [21] J. A. T. Machado, A. M. Lopes, Rare and extreme events: the case of COVID-19 pandemic, *Nonlinear Dynamics* (2020). doi:10.1007/s11071-020-05680-w.
- [22] N. James, M. Menzies, Cluster-based dual evolution for multivariate time series: Analyzing COVID-19, *Chaos: An Interdisciplinary Journal of Nonlinear Science* 30 (2020) 061108. doi:10.1063/5.0013156.
- [23] B. Blasius, Power-law distribution in the number of confirmed COVID-19 cases, *Chaos: An Interdisciplinary Journal of Nonlinear Science* 30 (2020) 093123. doi:10.1063/5.0013031.
- [24] M. Perc, N. G. Miksić, M. Slavinec, A. Stožer, Forecasting COVID-19, *Frontiers in Physics* 8 (2020) 127. doi:10.3389/fphy.2020.00127.
- [25] K. Shang, B. Yang, J. M. Moore, Q. Ji, M. Small, Growing networks with communities: A distributive link model, *Chaos: An Interdisciplinary Journal of Nonlinear Science* 30 (2020) 041101. doi:10.1063/5.0007422.
- [26] A. Karaivanov, A social network model of COVID-19, *PLOS ONE* 15 (2020) e0240878. doi:10.1371/journal.pone.0240878.
- [27] R. Moeckel, B. Murray, Measuring the distance between time series, *Physica D: Nonlinear Phenomena* 102 (1997) 187–194. doi:10.1016/s0167-2789(96)00154-6.
- [28] G. J. Székely, M. L. Rizzo, N. K. Bakirov, Measuring and testing dependence by correlation of distances, *The Annals of Statistics* 35 (2007) 2769–2794. doi:10.1214/009053607000000505.

- [29] C. F. Mendes, M. W. Beims, Distance correlation detecting Lyapunov instabilities, noise-induced escape times and mixing, *Physica A: Statistical Mechanics and its Applications* 512 (2018) 721–730. doi:10.1016/j.physa.2018.08.028.
- [30] C. F. O. Mendes, R. M. da Silva, M. W. Beims, Decay of the distance autocorrelation and Lyapunov exponents, *Physical Review E* 99 (2019). doi:10.1103/physreve.99.062206.
- [31] A. Vazquez, Polynomial growth in branching processes with diverging reproductive number, *Physical Review Letters* 96 (2006). doi:10.1103/physrevlett.96.038702.
- [32] J. H. Ward, Hierarchical grouping to optimize an objective function, *Journal of the American Statistical Association* 58 (1963) 236–244. doi:10.1080/01621459.1963.10500845.
- [33] G. J. Szekely, M. L. Rizzo, Hierarchical clustering via joint between-within distances: Extending Ward’s minimum variance method, *Journal of Classification* 22 (2005) 151–183. doi:10.1007/s00357-005-0012-9.
- [34] A.-M. Madore, et al., Contribution of hierarchical clustering techniques to the modeling of the geographic distribution of genetic polymorphisms associated with chronic inflammatory diseases in the Québec population, *Public Health Genomics* 10 (2007) 218–226. doi:10.1159/000106560.
- [35] M. Kretzschmar, R. T. Mikolajczyk, Contact profiles in eight European countries and implications for modelling the spread of airborne infectious diseases, *PLoS ONE* 4 (2009) e5931. doi:10.1371/journal.pone.0005931.
- [36] H. Alashwal, M. E. Halaby, J. J. Crouse, A. Abdalla, A. A. Moustafa, The application of unsupervised clustering methods to Alzheimer’s disease, *Frontiers in Computational Neuroscience* 13 (2019). doi:10.3389/fncom.2019.00031.
- [37] H. Muradi, A. Bustamam, D. Lestari, Application of hierarchical clustering ordered partitioning and collapsing hybrid in Ebola virus phylogenetic analysis, in: 2015 International Conference on Advanced Computer Science and Information Systems (ICACSIS), IEEE, 2015, pp. 317–323. doi:10.1109/icacsis.2015.7415183.
- [38] R. Rizzi, P. Mahata, L. Mathieson, P. Moscato, Hierarchical clustering using the arithmetic-harmonic cut: Complexity and experiments, *PLoS ONE* 5 (2010) e14067. doi:10.1371/journal.pone.0014067.
- [39] N. James, M. Menzies, L. Azizi, J. Chan, Novel semi-metrics for multivariate change point analysis and anomaly detection, *Physica D: Nonlinear Phenomena* 412 (2020) 132636. doi:10.1016/j.physd.2020.132636.

- [40] D. J. Fenn, M. A. Porter, S. Williams, M. McDonald, N. F. Johnson, N. S. Jones, Temporal evolution of financial-market correlations, *Physical Review E* 84 (2011). doi:10.1103/physreve.84.026109.
- [41] W. Rudin, *Functional Analysis*, McGraw-Hill Science, 1991.
- [42] Human development reports, <http://hdr.undp.org/en/content/human-development-index-hdi>, 2020. United Nations Development Programme.
- [43] N. James, M. Menzies, P. Radchenko, COVID-19 second wave mortality in Europe and the United States, arXiv:2012.13197 (2020).
- [44] Sweden adds further restrictions on outdoor gatherings as coronavirus cases hit record highs, <https://www.abc.net.au/news/2020-11-17/12891116>, 2020. ABC, November 17, 2020.
- [45] S. Neuman, France announces further reopening amid declining number of coronavirus cases, <https://www.npr.org/sections/coronavirus-live-updates/2020/06/15/876953360>, 2020. NPR, June 15, 2020.
- [46] A. Boadle, Brazil has record new coronavirus cases, surpasses France in deaths, <https://www.reuters.com/article/idUSKBN2360U8>, 2020. Reuters, May 31, 2020.
- [47] C. Kantis, S. Kiernan, J. S. Bardi, Updated: Timeline of the Coronavirus, <https://www.thinkglobalhealth.org/article/updated-timeline-coronavirus>, 2020. Think Global Health, December 31, 2020.
- [48] Our World in Data, <https://ourworldindata.org/coronavirus-source-data>, 2020. Accessed November 25, 2020.
- [49] S. A. Lauer, et al., The incubation period of Coronavirus disease 2019 (COVID-19) from publicly reported confirmed cases: Estimation and application, *Annals of Internal Medicine* 172 (2020) 577–582. doi:10.7326/m20-0504.